Industrial Crops & Products 220 (2024) 119242

Contents lists available at ScienceDirect

Industrial Crops & Products

journal homepage: www.elsevier.com/locate/indcrop

From invasive species to bio-based composites: Utilizing water hyacinth for sound absorption and insulation

Maenila Srisawas [a], Thanate Kerdkaew [b], Purintorn Chanlert [a,*]

[a] Program of Physics, Faculty of Science and Technology, Songkhla Rajabhat University, Mueang, Songkhla 90000, Thailand
[b] Chemistry and Biology Unit, The Institute for the Promotion of Teaching Science and Technology, Klong Toei, Bangkok 10110, Thailand

ARTICLE INFO

Keywords:
Water hyacinth
Bio-based materials
Sound absorption coefficient
Sound transmission loss
Porous materials
Sustainable materials

ABSTRACT

This study evaluates the acoustic properties of water hyacinth fiber composites, a notorious invasive species, focusing on their effectiveness as sound absorbers and insulators. By converting this abundant weed into bio-based materials, the research presents a promising eco-friendly alternative for acoustic applications. By examining a range of densities from 118 to 282 kg/m^3, the study identifies how density impacts the Sound Absorption Coefficient (SAC) and Transmission Loss (TL). Notably, the sample with a density of 118 kg/m^3 exhibited the highest Sound Absorption Average (SAA) at 0.63, while the densest sample at 282 kg/m^3 achieved the highest Transmission Loss Average (TLA) at 32.5 dB, illustrating a direct correlation between increased density and enhanced TL, alongside a decrease in SAC. Statistical models obtained from the analysis of variance (ANOVA), semi-phenomenological model (Johnson-Champoux-Allard (JCA) model), and empirical model (based on the Delany-Bazley model) have been developed to predict the sound absorption and sound insulation performance of water hyacinth. These models demonstrate average errors of 0.0300, 0.0346, and 0.0377, respectively, significantly outperforming established models like the Delany-Bazley and Garai-Pompoli models in predicting the sound absorption average of water hyacinth bio-based composites. These models can be used to predict the acoustic properties of the composites, assisting in tailoring the composites to match specific applications. This approach leverages the natural abundance of water hyacinth to develop environmentally friendly acoustic materials, offering a sustainable solution to invasive species management and material development.

1. Introduction

Environmental noise pollution can profoundly impact human health and well-being, giving rise to some health issues including physical and psychological aspects. Historically, synthetic acoustic materials, such as mineral wools (Uris et al., 1999), were used widespread due to their commendable sound absorption characteristics. However, their utilization presents health concerns, stemming from the presence of harmful chemicals that can provoke respiratory ailments (Kudo et al., 2009). While glass wool represents a more environmentally acceptable alternative such as natural fibers (Aso and Kinoshita, 1965; Lei et al., 2018; Yang et al., 2017) or recycled materials (Dehdashti et al., 2024), it still entails adverse long-term ecological consequences.

Consequently, there has been a growing surge of interest in exploring natural acoustic materials as a promising avenue for addressing these challenges. Numerous natural fibers, including kapok (Xiang et al., 2013), coconut coir (Hosseini Fouladi et al., 2010; Taban et al., 2019), luffa (Halashi et al., 2024), waste corn husk (Fattahi et al., 2023) and other fibers made from palm type plants such as date palm (Taban et al., 2021) palmyra palm (Chanlert et al., 2022b), nipa palm (Chanlert et al., 2024) etc., have been subjected to extensive investigation regarding their acoustic absorption properties. One interesting approach is to incorporate natural fibers into a synthetic material matrix. For instance, adding kenaf fiber to elastic polyurethane foam enhances the sound absorption performance of the foam (Ehsan Samaei et al., 2023). The presence of the fiber alters the pore size of the foam, contributing to improved acoustic properties (Sukhawipat et al., 2022).

Invasive species pose a significant threat to global biodiversity and human well-being (Pejchar and Mooney, 2009). They disrupt native ecosystems through competition, predation, and the transmission of diseases and parasites to indigenous species (Hulme et al., 2010). These species also impact various economic sectors, including agriculture and aquaculture, and are notoriously difficult and costly to control (Marbuah et al., 2014). One such species, *Pontederia crassipes* Mart., known as

* Correspondence to: Faculty of Science and Technology, Songkhla Rajabhat University, Mueang, Songkhla 90000, Thailand.
E-mail address: purintorn.ch@skru.ac.th (P. Chanlert).

https://doi.org/10.1016/j.indcrop.2024.119242
Received 1 May 2024; Received in revised form 29 June 2024; Accepted 15 July 2024
Available online 29 July 2024

water hyacinth, is commonly found in several Thailand's water bodies. It proliferates rapidly, covering water surfaces and blocking sunlight and nutrients from reaching the water below. This dense coverage diminishes water flow, especially in canals, leading to increased flooding risks (Viriyavisuthisakul et al., 2018). Consequently, the Thai government annually spends over 300 million baht (approximately 8.5 million USD) on the removal of aquatic weeds, primarily water hyacinth, to improve water quality and mitigate flood risks (Royal Irrigation Department of Thailand, 2023).

Moreover, various initiatives are investigating the use of water hyacinth for producing fertilizer, fuel, bioplastics, bioethanol, and composite materials, potentially aiding in population control (Sierra-Carmona et al., 2022). Despite these applications, managing the spread of water hyacinth remains a formidable challenge. The plant's structure and anatomy, featuring numerous gas-filled spaces, enables it to float (Mahmood et al., 2005). Additionally, its fibrous structure may be transformed into a porous material with sound-absorbing properties. This trait suggests potential benefits in reducing noise pollution, which is favorable for both environmental and public health.

This paper encompasses the following in both sound insulation and sound absorption aspects of water hyacinth composites. Sound insulation materials serve to block external noise, while acoustic absorption materials are designed to attenuate internal noises including echoes and reverberation (Allard and Atalla, 2009). In this paper, materials and methods section comprehensively details the materials and methodologies employed in the fabrication of an composites utilizing water hyacinth fiber. For results and discussions section, the acoustic measurements are presented, encompassing the sound absorption coefficient (SAC) and transmission loss (TL) spectra. The Johnson-Champoux-Allard (JCA) model (Allard and Champoux, 1992; Champoux and Allard, 1991; Champoux and Stinson, 1992; Johnson et al., 1987, 1986) is utilized to analyze the non-acoustic parameters that exert influence on the SAC and TL properties of the material. Statistical (Ehsan Samaei et al., 2023; Mehrzad et al., 2022) and empirical (Berardi and Iannace, 2017; Chanlert et al., 2024, 2023; Delany and Bazley, 1970; Ehsan Samaei et al., 2023) models were also studied with the aim of creating tools to help predict acoustic properties from non-acoustic parameters such as density and airflow resistivity. In the conclusion section, we summarize the findings and engage in a thorough exploration of the potential applications of water hyacinth as an acoustic material, underscoring its environmental and sustainability benefits.

2. Materials and methods

2.1. Sample preparation

This section describes the preparation of cylindrical samples using water hyacinth (WH) fibers sourced from a local canal in Songkhla province, Thailand. All water hyacinth stems were collected from one population in the same natural habitat (the same canal) to avoid variability due to different locations. The process involved using fresh plant's central stem, discarding the leaves, and breaking it down with mallet into rough fibers of approximately 1–2 mm in diameter. These fibers were sun-dried for 3 days and then further dried in an air-circulating oven at 90 °C for two hours to remove moisture, crucial for preventing weighing inaccuracies. After drying, the fibers were stored in a humidity-controlled cabinet at 40 %RH for a minimum of 24 hours before further processing. The fibers were cut into 40 mm lengths for composite materials with fiber content ranging from 3 g to 7 g per controlled volume, labeled WH-1 to WH-5. A sample size of 3 was used for each treatment. A 10 % polyvinyl alcohol (PVA) binder was used to hold the fibers, which were then mixed with the binder and cast into cylindrical molds of 28.6 mm diameter and 40.0 mm thickness, ensuring random fiber orientation. Sufficient pressure was applied to prevent overflow, and the mixture set in molds for 24 hours followed by a 30-minute heat treatment at 90 °C. After demolding, samples underwent a 60-minute drying in an air-circulating oven at 90 °C, then stored in a dry cabinet at 40 %RH for at least 24 hours before further analysis. A detailed flowchart of the process is provided in Fig. 1. The process was strictly regulated to ensure that each sample contained the same amount of WH, with a density variation not exceeding 10 %, as the density of a porous absorber significantly influences airflow resistivity (Garai and Pompoli, 2005). Furthermore, airflow resistivity, which greatly impacts sound absorption property especially the sound absorption coefficient (Delany and Bazley, 1970), was maintained within a 15 % error margin. Samples that did not meet these criteria were excluded from acoustic property measurements to avoid potential inconsistencies.

To investigate the microscopic examinations of the water hyacinth fibers, the fiber surfaces (cross-sectional and longitudinal) were examined using a field-emission scanning electron microscope (FEG-SEM, Phenom Pharos G2, Thermo Fisher Scientific, UK).

2.2. Airflow resistivity measurement

Airflow resistivity (σ) is a crucial parameter for understanding the sound absorption of porous materials, measuring their resistance to air flow. The determination of σ followed the ISO-9053 standard (ISO-9053-1–1., 2018) consistent with methods from our prior research (Chanlert et al., 2024, 2023). The equation used for calculating airflow resistivity is outlined below:

$$\sigma = \left(\frac{A}{Qd}\right)\Delta P \tag{1}$$

where A signifies the sample cross-sectional area, d designates the thickness of the material, and ΔP is the pressure difference across the material. The schematic diagram of airflow resistivity measurement is shown in Fig. 2, and the obtained results are reported in Table 1 and graphically illustrated Fig. 8.

2.3. Sound absorption measurement

In this study, we followed the experimental setup of our previous works (Chanlert et al., 2023, 2022b) to measure the sound absorption coefficient (SAC) spectra using a custom-built impedance tube. This tube adheres to ISO-10534 (ISO-10534, 1998) and ASTM-E1050 (ASTM-E1050, 1990) standards using the transfer function method. The tube, with a 28.6 mm diameter and made of stainless steel to minimize background noise, incorporated two precision laboratory-grade measurement microphones (GRAS 46BD-FV, GRAS Sound & Vibration, Skovlytoften, Denmark) positioned and hermetically sealed against the tube's inner wall. A wideband noise source was generated utilizing a full-range speaker positioned at the terminus of the tube to generate planar sound waves directed toward the sample's surface. The schematic diagram of impedance tube diagram for sound absorption measurement is illustrated in Fig. 3.

The cylindrical sample was securely positioned within the sample holder at the opposing end of the tube, complemented by the placement of a rigid backing plate situated behind the sample. Signals emanating from the two microphones were systematically acquired through a data acquisition device (NI-9230 and cDAQ-9174, National Instrument, TX, USA) using Python. To ensure the reliability and alignment of the least-squares optimized parameters with the SAC spectra results across all air gap configurations (0 mm, 20 mm, and 40 mm), SAC spectra were systematically acquired for each of these configurations.

2.4. Transmission loss measurement

Sound insulation properties of the materials were assessed, relying on the transmission loss (TL). TL quantifies the reduction in sound intensity as it traverses a specified material or structure, with higher TL values signifying superior sound insulation (Ehrig et al., 2020; Golzari

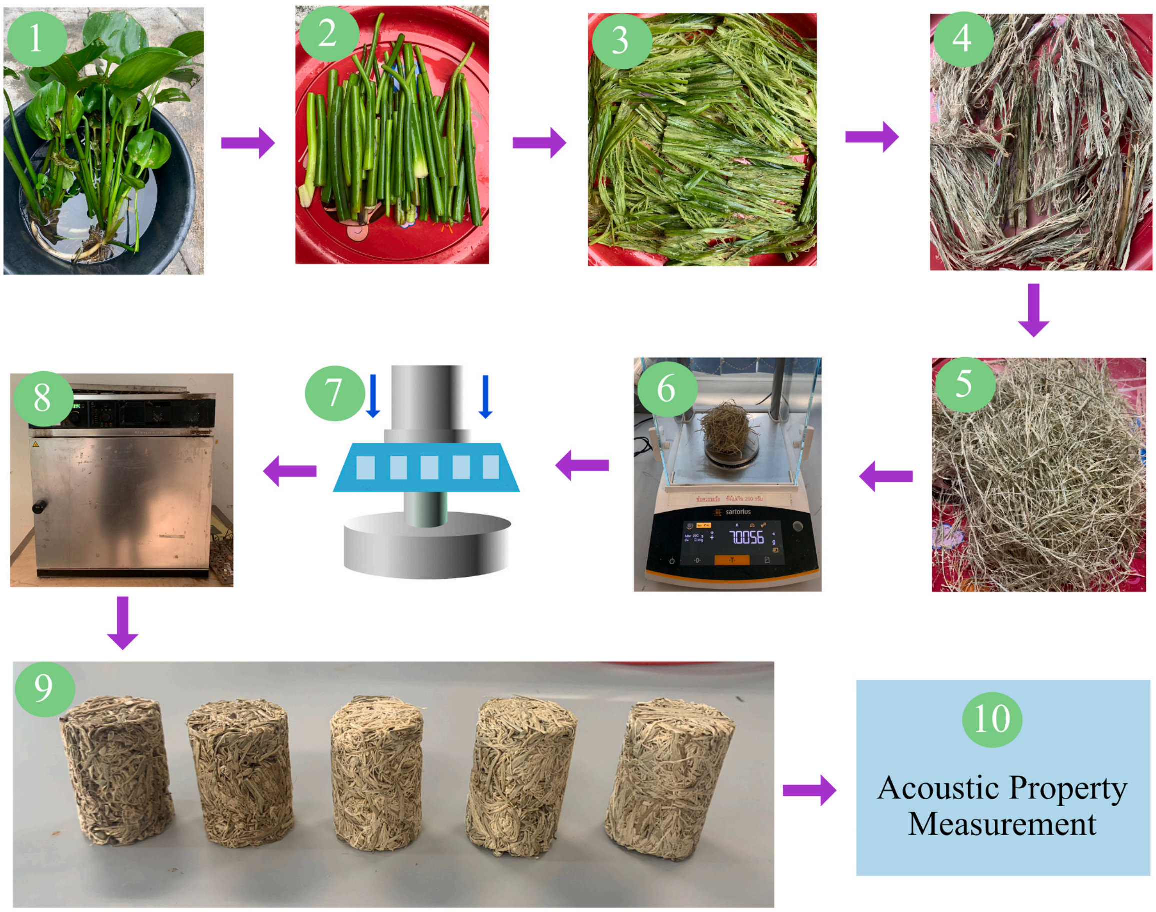

Fig. 1. Step-by-step preparation of water hyacinth (WH) composite samples: (1–5) drying WH fibers from fresh stalks; (6–8) pressing fibers into cylindrical molds and heat-treating; (9–10) producing cylindrical samples ready for acoustic testing.

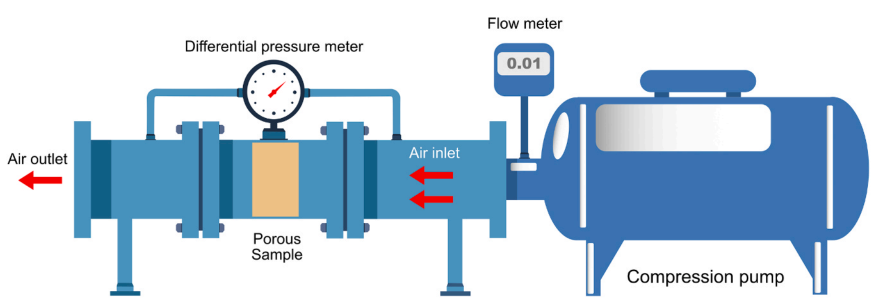

Fig. 2. Schematic diagram of airflow resistivity measurement system.

Table 1
Density, airflow resistivity, sound absorption average (SAA) with 0, 20 and 40 mm air gaps, and transmission loss average (TLA) of water hyacinth samples.

Sample	ρ (kg/m^3)	σ (Pa·s·m^{-2})	SAA	SAA$_{(20)}$	SAA$_{(40)}$	TLA (dB)
WH-1	118(4)	2824(290)	0.63(0.01)	0.72(0.02)	0.76(0.01)	7.5(1.0)
WH-2	174(5)	15920(728)	0.59(0.02)	0.68(0.02)	0.72(0.03)	11.2(0.9)
WH-3	197(2)	42061(4022)	0.58(0.04)	0.62(0.05)	0.61(0.06)	14.3(4.2)
WH-4	240(3)	62038(2191)	0.56(0.02)	0.59(0.03)	0.61(0.04)	17.5(2.9)
WH-5	282(2)	134251(4925)	0.41(0.01)	0.40(0.01)	0.40(0.01)	32.5(1.4)

The value in parentheses contains the standard deviation (SD) of each measurement.

and Jafari, 2018). TL measurements were conducted employing a domestically constructed four-microphone impedance tube (Chanlert et al., 2024, 2022b), designed to adhere to the ASTM-E2611 standard (ASTM-E2611., 2019) where the transfer matrix method was employed (Cai et al., 2015; Chanlert et al., 2024; Doutres et al., 2015). The schematic diagram of impedance tube diagram for sound transmission loss is shown in Fig. 4. In elucidating the acoustic insulation characteristics of the porous fibrous composites, the semi-phenomenological

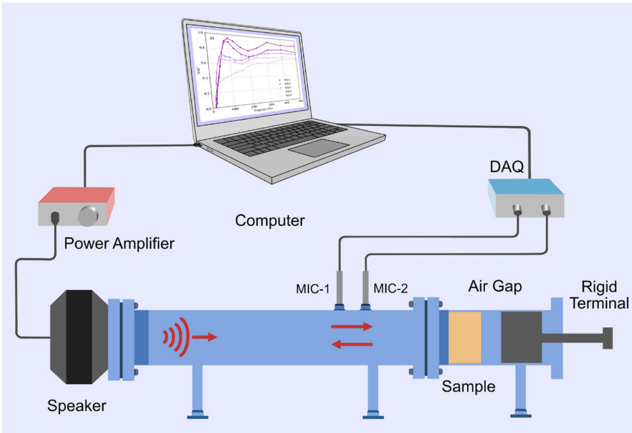

Fig. 3. Two-microphone impedance tube diagram for sound absorption measurement.

Johnson-Champoux-Allard (JCA) model has been utilized, following a similar approach to our treatment of SAC data as presented in results and discussions section.

The analysis of variance (ANOVA) using quadratic model was used to determine the significance of the independent variables and their interactions on the response (SAA and TLA). The analysis was determined using the 'statsmodels' library in Python.

3. Results and discussions

3.1. Characteristics of water hyacinth bio-based composites

The water hyacinth (WH) fiber strands used in this study displayed a characteristic roughness, with an average diameter spanning from 1 to 2 mm. As depicted in Fig. 5, the samples were casted into cylindrical shapes, featuring controlled dimensions for both diameter and thickness. Owing to the transparent nature of the PVA adhesive, the resulting samples naturally exhibited the characteristic light brown color of dried water hyacinth.

The SEM image of the longitudinal section, displayed in Fig. 5(a), highlights that a single strand of coarse fiber, acquired exclusively through mechanical means, comprises smaller, unextracted strands. The chemical composition of water hyacinth fiber mostly consists of cellulose (25–68 %), hemicellulose (11–31 %), and lignin (3–7 %) (Guna et al., 2017; Tanpichai et al., 2019; Wembe et al., 2023). The variation in chemical composition may be affected by several abiotic factors, such as water temperature and climate, as well as biotic factors such as water hyacinth population density (Tanpichai et al., 2019). The chemical composition of WH fiber plays a crucial role in contributing to the strength of the fiber as described by Zhang et al. (2023) that lignin, a main component of wood cell walls, has a critical effect on the mechanical properties of paper pulp and wood fiber-based composites. Additionally, Oladele et al. (2020) showed that the lignin and hemicellulose contents in the fiber affect surface morphology, which ultimately can influence acoustic properties. Conversely, the analysis of the cross-section, as shown in Fig. 5(b), uncovers the inherent porous and fibrous structure of the cell wall, aligning with the typical features observed in specific aquatic plants. Notably, this porous structure is

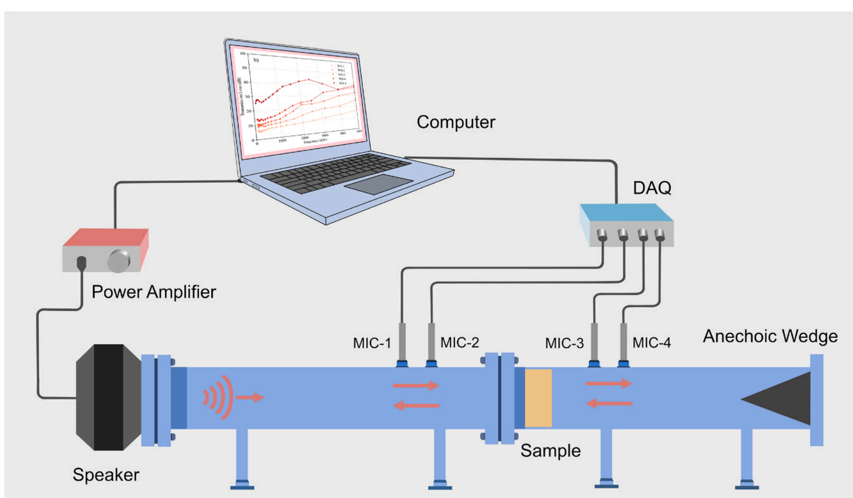

Fig. 4. Four-microphone impedance tube diagram for transmission loss measurement.

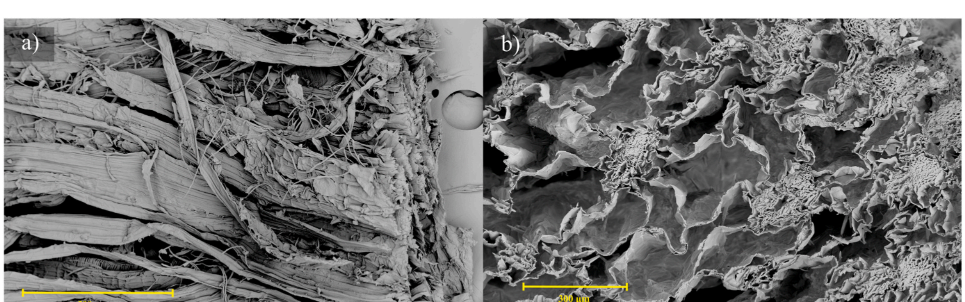

Fig. 5. FEG-SEM images of the a) longitudinal section and b) cross section of rough water hyacinth fiber strands.

reminiscent of the characteristics found in aquatic plants, notably the water hyacinth, where numerous air spaces are dispersed throughout its structure (Mahmood et al., 2005). There are two key morphological characteristics that affect the sound-absorbing properties of water hyacinth composites. Firstly, fiber diameter plays a crucial role. According to the study incorporating Kozeny-Carman model (Chanlert et al., 2022b; Pelegrinis et al., 2016), fiber diameter is one of the essential factors in determining the airflow resistivity of porous fibrous materials, which in turn influences their sound absorption properties. Smaller fiber diameters result in a higher specific surface area within the porous structure, leading to greater energy dissipation of sound waves traveling through the structure due to viscous and thermal effects. Secondly, fiber surface roughness also impacts sound absorption. Theoretically, increased surface roughness of the fiber enhances the surface area available for sound wave interaction, thereby promoting more friction and energy dissipation (Halashi et al., 2024; Mehrzad et al., 2022).

Fiber density plays a significant role in determining sound absorption properties. Low-density fibers create more space, resulting in acoustic panels with lower overall density. Additionally, for the same areal density, lower-density fibers provide a more voluminous and bulkier fibrous structure compared to higher-density fibers. As reported by Wembe et al. (Wembe et al., 2023), the density of water hyacinth fiber ranges from 1.23 to 1.45 g/cm^3, which is similar to other natural fibers such as kenaf (1.4 g/cm^3) (Taban et al., 2020), banana fiber (1.38 g/cm^3) (Oladele et al., 2020), and sisal fiber (1.45 g/cm^3) (Castoldi et al., 2019).

The density of each sample was systematically measured and is comprehensively presented in Table 1. It is noteworthy that as the water hyacinth fiber content in the samples increased, so did the sample density. The recorded sample densities ranged from 116 to 287 kg/m^3, a classification considered as medium density, in alignment with previous research findings incorporating natural fibers (Chanlert et al., 2022b; Taban et al., 2021, 2019).

Airflow resistivity results, as shown in Table 1 and illustrated in Fig. 8, exhibited a direct correlation with the sample density of the composites. Specifically, higher sample densities corresponded to elevated airflow resistivity values like the results from previous studies (Mehrzad et al., 2022; Soltani et al., 2020). The airflow resistivity of porous samples demonstrates an exponential relationship with sample density, as supported by both theoretical (Garai and Pompoli, 2005) and experimental (Chanlert et al., 2022b, 2023) evidence in previous studies.

3.2. Sound absorption and sound insulation properties

The Sound Absorption Coefficient (SAC) spectra provide insights into a sample's ability to absorb sound at various frequencies, with values ranging from 0 (no absorption) to 1 (full absorption). Fig. 6(a) presents the SAC spectra for water hyacinth fiber samples WH-1 through WH-5, obtained with the backing plate positioned directly behind the sample, ensuring zero air gap. A clear inverse correlation between the SACs and sample density emerges. This trend aligns with established characteristics of some porous absorbers, where low-density samples often show higher SACs (Chanlert et al., 2022b, 2022a). As the frequency rises, the SAC exponentially increases, plateauing in a saturation region (Simón-Herrero et al., 2019; Yang et al., 2020). Within this region, samples of lower densities, such as WH-1 and WH-2, display a peak-valley phenomenon, attributed to the 1/4-wavelength resonance of the material's rigid frame (Bardot et al., 1996). However, when the sample density is sufficiently high or the open porosity is too low, the peak-valley characteristic tends to disappear, as demonstrated in several previous studies (Chanlert et al., 2022a; Park et al., 2020). In this study, WH-5 exhibits such characteristic.

In Fig. 6(b), the transmission loss (TL) experimental data reveal a pronounced positive correlation with sample density, presenting an interesting contrast to the previously discussed SAC results. This trend starkly contrasts with the SACs, highlighting differing behaviors in sound absorption and transmission loss (Norton and Karczub, 2003). This behavior is similar to the prior study on palmyra palm fiber composites (Chanlert et al., 2022b), where the TL of porous fibrous absorbers with consistent thickness is significantly influenced by sample density. Notably, this empirical insight applies well to water hyacinth samples, given their classification as porous fibrous absorbers. In alignment with these observations, sample WH-1, which has the lowest density, exhibits the minimum transmission loss (TL), while WH-5, with its higher density, shows a corresponding increase. Most samples display a linear-like dependency of TL on frequency. However, sample WH-5 shows a nuanced deviation from this pattern; while the overall trend of increasing TL with frequency is maintained, a pronounced hump emerges between 125 and 4000 Hz. This feature intriguingly mirrors the SAC results for WH-5, where the typical peak-valley characteristic is conspicuously absent. Within the framework of water hyacinth porous fibrous composites, a pivotal trade-off becomes apparent: optimizing for superior SAC inevitably compromises TL, and vice versa.

Table 1 summarized key parameters for samples WH-1 through WH-5, showing a progressive increase in sample density (ρ) from 118 ± 4 kg/m^3 for WH-1–282 ± 2 kg/m^3 for WH-5. The Sound Absorption Average (SAA) is calculated by averaging SAC values across specific 1/3 octave-band frequencies between 200 and 2500 Hz, following previously established methodologies (Chanlert et al., 2022b). There is an evident inverse correlation between sample density and SAA, with values decreasing from 0.63 to 0.41. This trend aligns with the SAC spectra; for instance, WH-5, with its higher density, lacks pronounced peak-valley characteristics, which is reflected in its lower SAA. The data

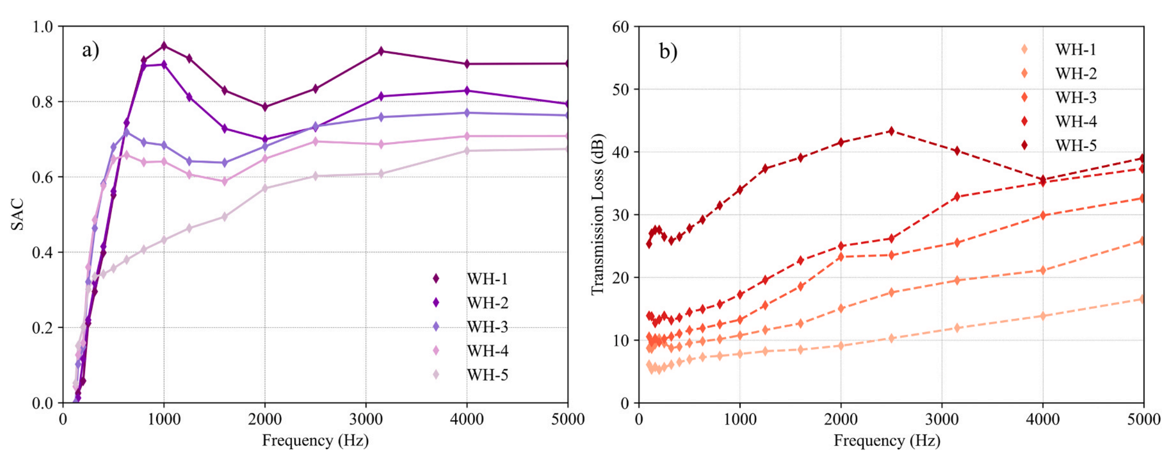

Fig. 6. Normal-incident a) SAC and b) transmission loss (TL) spectra of water hyacinth bio-based composites.

highlights the inverse relationship between SAC and sample density, showing how density affects the acoustic properties of water hyacinth samples. In the same way, The Transmission Loss Average (TLA) was calculated using the same approach as the SAA, considering TL values at 1/3 octave-band frequencies between 200 and 2500 Hz. TLA demonstrates a direct relationship with sample density, where WH-1 exhibits the lowest TLA at 7.5 dB and WH-5 the highest at 32.5 dB. TLA values of all samples are shown in Table 1. Fig. 8(f) illustrates the graphical demonstration of SAA and TLA. It is evident that SAA tends to decrease with increasing sample density, while TLA exhibits the opposite behavior, with higher sample density corresponding to higher TLA.

3.3. Effect of air gap on sound absorption

Introducing an air space behind the porous absorber is a simple and cost-effective way to boost sound absorption, especially at lower frequencies (Halashi et al., 2024). From Table 1, it is evident that the SAA of the samples increases significantly for those with lower densities (<240 kg/m^3). As illustrated in Fig. 7, the SAC spectra for low-density samples show a shift in the peak SAC towards lower frequencies. For the densest sample, WH-5 (282 kg/m^3), the impact of the air gap is minimal. This is probably because this sample behaves more like a solid than a porous material due to its low porosity and high airflow resistivity as displayed in Table 3.

The depth of the air gap is crucial in enhancing sound absorption. Increasing the air gap depth leads to a marked improvement in low-frequency sound absorption. This enhancement is attributed to the additional sound energy dissipation as sound waves travel through the air gap through the Helmholtz resonance effect (Chanlert et al., 2024; Halashi et al., 2024). By adjusting the air gap depth, it is possible to control the resonant frequency and improve sound absorption at specific frequencies. Furthermore, increasing the air gap depth shifts the absorption peak to lower frequencies, indicating that maximum absorption occurs at these lower ranges. For instance, in Table 1, WH-1 sample with a thickness of 40 mm and a density of 118 kg/m^3 without an air gap has an SAA of 0.63. Introducing air gaps of 20 mm and 40 mm increases the SAA to 0.72 and 0.76, respectively. Thinner-porous samples, which typically have lower SAA, can achieve similar performance to thicker samples by incorporating an air gap (Halashi et al., 2024). From Fig. 7, it is observed that the absorption peaks shift to lower frequencies, resulting in a decrease in SAC at higher frequencies (Chanlert et al., 2024, 2023; Halashi et al., 2024). This indicates that enhancing SAC at lower frequencies through the use of an air gap necessitates a trade-off in sound absorption performance at higher frequencies. Therefore, optimizing acoustic panels with an air gap is crucial to achieve the desired sound absorption levels for specific applications (Merve Küçükali Öztürk and Cevza Candan., 2015; Mvubu et al., 2019).

3.4. Analysis of variance (ANOVA) of factors affecting acoustic properties

The effects of sample density (kg/m^3) and air gap (mm) on the sound absorption average (SAA) were investigated using ANOVA with a quadratic model (Ehsan Samaei et al., 2023; Mehrzad et al., 2022). For the Sound Absorption Average (SAA), the independent variable X represents the linear effect of sample density, while Y denotes the linear effect of the air gap, which includes 0, 20, and 40 mm. The variables X^2 and Y^2 represent the quadratic effects of sample density and air gap, respectively, and XY represents their interaction. For the Transmission Loss Average (TLA), sample density is the only independent variable considered. Here, X and X^2 represent the linear and quadratic effects of sample density, respectively.

After performing the quadratic ANOVA test, the following mathematical model (Eq.2) was derived to predict the SAA:

$$SAA = 0.4194 + 2.951 \times 10^{-3}X + 7.850 \times 10^{-3}Y - 1.054 \times 10^{-5}X^2 - 4.408 \times 10^{-5}Y^2 - 2.176 \times 10^{-5}XY \quad (2)$$

The ANOVA findings demonstrated that the model was highly significant with an F-value of 81.27 and a p-value of 1.11 × 10^{-16}. The coefficients of determination R^2 and adjusted R^2 of were 0.91 and 0.90, respectively, indicating a strong agreement between the model and the experimental data. The mean SAA was 0.59, with a standard deviation of 0.11, resulting in a coefficient of variation (CV) of 0.19. These statistical

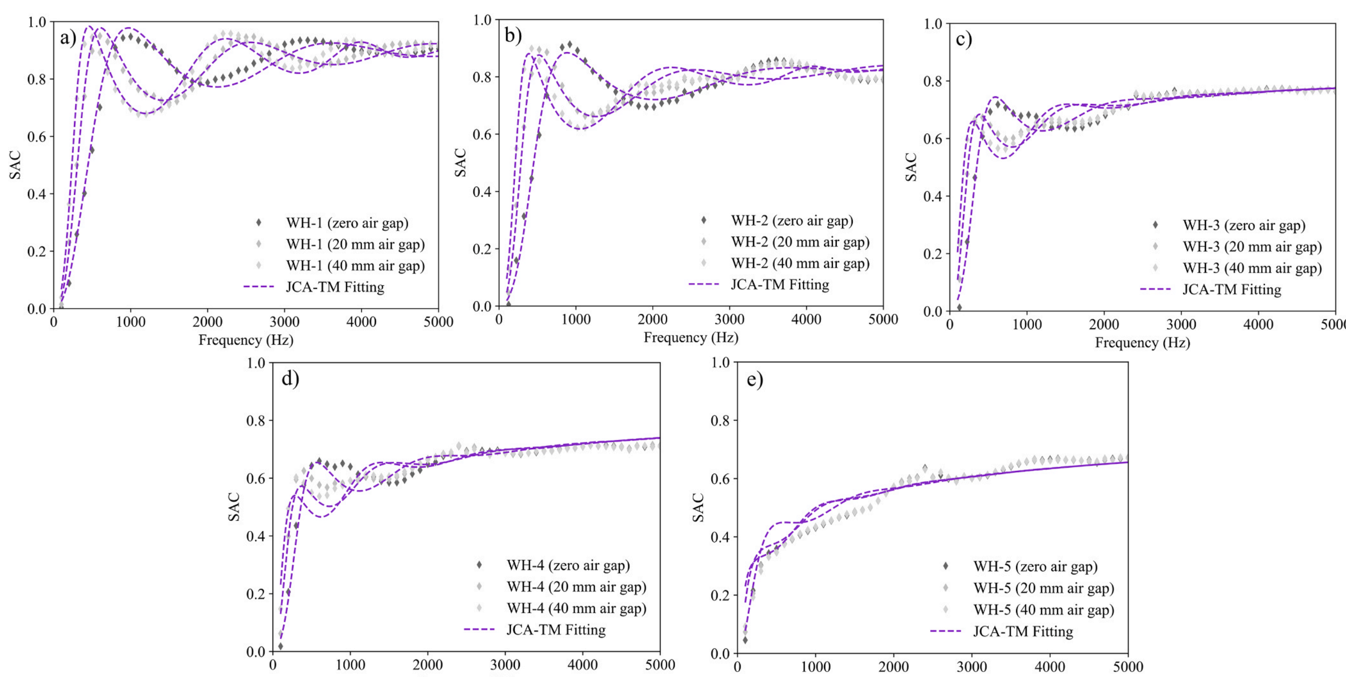

Fig. 7. SAC spectra measured with 0, 20, and 40 mm air gaps and estimation curves obtained from the JCA model for a) WH-1, b) WH-2, c) WH-3, d) WH-4, and e) WH-5.

parameters confirm the adequacy and reliability of the model for predicting the SAA of the composite materials. The significant terms in the model included the linear effects of density (X) and air gap (Y), as well as their interaction (XY) and the quadratic term of density (X^2). The quadratic term of air gap (Y^2) was not significant at the 95 % confidence level (p-value = 0.125).

The error analysis was conducted to assess the experimental outcomes against the prediction using statistical model. The errors between experimental (A_{exp}) and predicted (A_{model}) values for each sample were calculated by following (Eq. 3 ~ Eq. 4):

$$\text{residual} = |A_{exp} - A_{model}| \tag{3}$$

$$\text{error} = \text{residual}/A_{exp} \tag{4}$$

where residual is the absolute difference between the experimental and predicted values.

The results indicate that both density and air gap significantly affect the SAA, with density exerting a more pronounced influence. The errors in the mathematical model's predictions for SAA with zero air gap, SAA with a 20 mm air gap ($SAA_{(20)}$), and SAA with a 40 mm air gap ($SAA_{(40)}$) are 0.0300, 0.1892, and 0.2074, respectively. These findings demonstrate that the mathematical model exhibits higher accuracy in predicting SAA without an air gap compared to predictions involving 20 mm and 40 mm air gaps.

The influence of sample density (kg/m^3) on the Transmission Loss Average (TLA) was analyzed using a quadratic model. The ANOVA results, as summarized in Table 2, confirmed the model's high significance (F-value = 74.46, p-value = 1.72×10^{-7}). The derived mathematical model (Eq.5) for predicting TLA is:

$$TLA = 22.34 - 0.2326X + 9.386 \times 10^{-4}X^2 \tag{5}$$

The analysis demonstrated a strong correlation between the model and experimental data, indicated by an R^2 value of 0.93 and an adjusted R^2 of 0.91. The model terms, including the linear effect of density (X) and the quadratic term (X^2), were statistically significant at 95 % confidence level with p-values of 0.0292 and 1.65×10^{-3}, respectively. Key statistical parameters further validated the model's reliability: the mean TLA was 16.6, with a standard deviation of 9.2, resulting in a coefficient of variation (CV) of 0.55. These findings indicate that sample density significantly affects TLA, with the model providing a highly accurate prediction of the transmission loss average. The error of this quadratic math model in predicting TLA is 0.0886.

The next subsection introduces the semi-phenomenal Johnson-Champoux-Allard (JCA) model, which could help explain these interactions. The JCA model enables deeper exploration into the relationship between SAC and TL in water hyacinth composites, potentially clarifying the complexities observed in experimental findings.

3.5. The analyses of Johnson-Champoux-Allard (JCA) model and transfer matrix method

The non-acoustic parameters constitute the geometric elements of the semi-phenomenal Johnson-Champoux-Allard (JCA) equivalent fluid model, as originally proposed by Johnson et al. (Johnson et al., 1987), Allard and Champoux (Allard and Champoux, 1992), and Champoux and Stinson (Champoux and Stinson, 1992). These parameters include airflow resistivity (σ), porosity (ϕ), tortuosity (α_∞), viscous (Λ), and thermal (Λ') characteristic lengths. The expressions for the equivalent dynamic density and equivalent dynamic bulk modulus governing the behavior of airborne sound waves within the porous absorber are presented below (Chanlert et al., 2024, 2023, 2022b):

$$\rho_{eq}(\omega) = \frac{\alpha_\infty \rho_0}{\phi}\left[1 + \frac{\sigma\phi}{j\omega\rho_0\alpha_\infty}\left(1 + \frac{4j\alpha_\infty^2\eta\omega\rho_0}{(\sigma\Lambda\phi)^2}\right)^{1/2}\right] \tag{6}$$

$$K_{eq}(\omega) = \frac{\gamma P_0}{\phi}\left(\gamma - (\gamma - 1)\left[1 + \frac{\sigma\phi}{j\omega\rho_0\alpha_\infty N_{PR}}\left(1 + \frac{4j\alpha_\infty^2\eta N_{PR}\omega\rho_0}{(\sigma'\Lambda'\phi)^2}\right)^{1/2}\right]^{-1}\right)^{-1} \tag{7}$$

$$\sigma' = \frac{8\eta\alpha_\infty}{\Lambda'^2\phi} \tag{8}$$

where ω represents the angular frequency of the sound wave, ρ_0 denotes the density of the ambient air, γ signifies the specific heat ratio of the air, η corresponds to the dynamic viscosity of the air, P_0 stands for atmospheric pressure, and N_{PR} denotes the Prandtl number. The complex wave number (k_c) and characteristic impedance (Z_c) can be calculate through the following expressions:

$$k_c(\omega) = \omega\sqrt{\frac{\rho_{eq}(\omega)}{K_{eq}(\omega)}} \tag{9}$$

$$Z_c(\omega) = \sqrt{\rho_{eq}(\omega)K_{eq}(\omega)} \tag{10}$$

The transfer matrix (T) (Cai et al., 2020; Chanlert et al., 2023; Doutres et al., 2015) can be expressed as follows:

$$T = \begin{bmatrix} \cos(ka) & jZ\sin(ka) \\ j\sin(ka)/Z & \cos(ka) \end{bmatrix} \tag{11}$$

Table 2
Analysis of variance (ANOVA) for sound absorption average (SAA) and transmission loss average (TLA).

Response	Model	ANOVA					
		Source	Sum of square	DF	Mean square	F-value	p-value
SAA	Quadratic	Model	0.513	5	0.103	81.27	1.11×10^{-16}
		X	0.413	1	0.413	326.85	2.13×10^{-4}
		Y	343×10^{-2}	1	3.43×10^{-2}	27.18	2.76×10^{-5}
		XY	1.79×10^{-2}	1	1.79×10^{-2}	14.17	5.51×10^{-4}
		X^2	4.51×10^{-2}	1	4.51×10^{-2}	35.68	5.64×10^{-7}
		Y^2	3.11×10^{-3}	1	3.11×10^{-3}	2.46	0.125
		Residual	4.93×10^{-2}	39	1.26×10^{-3}	1.00	
		Total	0.563	44			
Statistical parameters (Mean = 0.59, SD = 0.11, CV = 0.19, R^2 = 0.91, R^2_{adj} = 0.90)							
TLA	Quadratic	Model	1089.12	2	544.56	74.46	1.72×10^{-7}
		X	970.03	1	970.03	132.64	0.0292
		X^2	119.09	1	119.09	16.28	1.65×10^{-3}
		Residual	87.76	12	7.31	1.00	
		Total	1176.88	14			
Statistical parameters (Mean = 16.6, SD = 9.2, CV = 0.55, R^2 = 0.93, R^2_{adj} = 0.91)							

$$T_{\text{total}} = \prod_{i=1}^{2} T_{\text{i}} = T_{\text{porous}} \bullet T_{\text{airgap}} = \begin{bmatrix} T_{11} & T_{12} \\ T_{21} & T_{22} \end{bmatrix} \tag{12}$$

For the porous and air layer, k can be substituted with complex wave number of the porous layer (k_c) and air (k_0), respectively. In the same way, Z can be substituted by characteristic impedance of porous absorber (Z_c) and air (Z_0). In addition, a signifies the thickness of the porous sample and the air gap layers. Lastly, the SAC of the composite system comprising the porous absorber and air layer can be expressed as follows:

$$\text{SAC} = 1 - \left| \frac{(T_{11}/T_{21}) - \rho_0 c_0}{(T_{11}/T_{21}) + \rho_0 c_0} \right|^2 \tag{13}$$

where ρ_0 and c_0 is the static density and sound speed of air at certain temperature, respectively.

The expression presented in Eq. 1 13)3 shall serve as the mathematical model for the least-squares fitting of SAC spectra for samples with air gaps of 0 mm, 20 mm, and 40 mm simultaneously. Fig. 7 shows the SAC results from the experiments alongside the fitting from the JCA model - transfer matrix. During the optimization process, airflow resistivity (σ) was kept constant as it was measured directly. Other parameters (ϕ, ε_0, Λ, and Λ') were treated as variables and optimized using the least-squares method by the 'lmfit' library in Python. The optimized non-acoustic parameters are listed in Table 1.

Fig. 7 compares the calculated and experimental SAC spectra for air gaps of 0, 20, and 40 mm. As the air gap length increases, a notable leftward shift in the SAC spectra indicates enhanced low-frequency sound absorption. Most samples' air gap variations align with predictions from the JCA model. However, according to Fig. 7(e), WH-5 is an exception, showing no low-frequency shift in its SAC spectrum. This behavior is similar to findings in high-density rice bran composites (Chanlert et al., 2023), where air gap variations minimally affected SAC. In such cases, higher sample density promotes rigidity, reducing the impact of air gap-induced frequency shifts.

According to Fig. 8, the variation between airflow resistivity and sample density is positive, where increasing sample density results in the airflow resistivity increase which is consistent with most porous materials in prior studies (Chanlert et al., 2024, 2022b). The results shown in Table 3 are visually demonstrated in Fig. 8. According to Garai and Pompoli (Garai and Pompoli, 2005), airflow resistivity can be determined by using sample density (ρ) as described in this empirical model:

Table 3
Non-acoustic parameters derived from a least-squares fiting of the JCA model on experimental sound absorption coefficient (SAC) spectra.

Sample	ϕ	α_∞	Λ (μm)	Λ' (μm)
WH-1	0.923	1.465	34.4	242.2
WH-2	0.803	1.000	15.3	179.0
WH-3	0.784	1.010	9.8	91.6
WH-4	0.716	1.052	9.1	26.7
WH-5	0.668	1.210	7.7	25.1

$$\sigma = A\rho^B \tag{14}$$

In the case of water hyacinth composites, by employing the least-squares method to optimize experimental airflow resistivity (σ) with Eq. (14), the parameters A and B, can be determined as 2.1651×10^{-5} and 3.9939, respectively. Using this empirical equation, the airflow resistivity of the water hyacinth sample can be determined. The model is capable of predicting the value of airflow resistivity based solely on sample density. The model's prediction exhibits an error of 0.2019. The estimation using Eq. (14) is illustrated in Fig. 8(a).

Table 3 shows the values of non-acoustic parameters obtained from the optimization of JCA model and experimental SACs results including opened porosity (ϕ), tortuosity (α_∞), viscous (Λ), and thermal (Λ') characteristic lengths. Most parameters (ϕ, ε_0, Λ, and Λ') exhibit approximately negative variation with sample density. Fig. 8 provides a detailed analysis of sample density against SAA, TLA and 5 non-acoustic parameters of JCA model across six subplots. Fig. 8(a) displays an exponential increase in airflow resistivity with density, where experimental and calculated data from Eq. 14 converge. Fig. 8(b) shows a linear decrease in open porosity as density increases. Tortuosity (α_∞), portrayed in Fig. 8(c), diminishes up to a sample density of 174 kg/m^3, subsequently stabilizing at a value indicative of straight, non-deviant pores. The viscous characteristic length, as depicted in Fig. 8(d), shows a decline with increasing density. Similarly, the thermal characteristic length also reveals an approximate decline with the increase in density. The underlying mechanisms, especially the interplay between α_∞, Λ, and Λ', suggest a hierarchy in pore characteristics: the Λ typically being smaller or at par with the Λ' (Champoux and Stinson, 1992), which

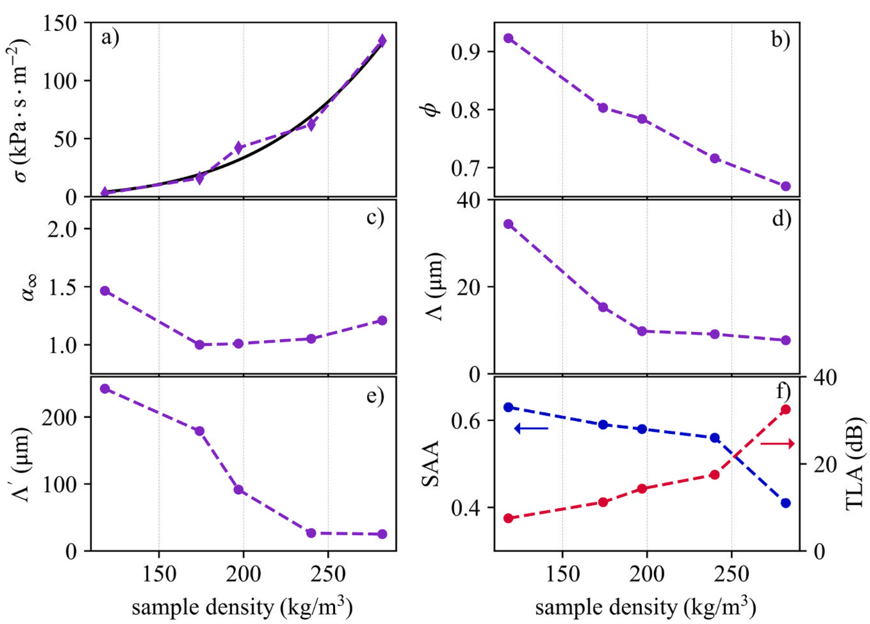

Fig. 8. Sample density vs a) airflow resistivity, b) opened porosity c) tortuosity, d) viscous characteristic length, e) thermal characteristic length, and f) SAA and TLA.

reveals complex pore geometry and connections within the porous absorber (Champoux and Allard, 1991).

Furthermore, the transmission loss (TL) can be determined using the matrix components of the transfer matrix (Chanlert et al., 2024; Luu et al., 2017) which is:

$$\mathrm{TL} = 20\log_{10}\left|\cos(k_c a) + \frac{i}{2}\left(\frac{Z_c}{\rho_0 c_0} + \frac{\rho_0 c_0}{Z_c}\right)\sin(k_c a)\right| \tag{15}$$

Using the above equation, calculated TL spectra can be determined. The caluculated TL spectra using JCA model and transfer matrix method are shown in Fig. 9. Notably, according to Fig. 6(e), the WH-4 and WH-5 samples exhibit disparities between the experimental and theoretical results. This observed discrepancy might be attributed to their high sample density and lowest opened porosity among the samples (Chanlert et al., 2022b). Given that Eq. 15 is utilized to determine TL for porous absorbers, the TL spectrum of high density sample deviating from the prediction might suggest that they behave more akin to a rigid material rather than a porous one (Chanlert et al., 2024, 2022b), which is consistent with the SAC results observed during air gap variation as demonstrated in Fig. 7.

The error analysis was conducted to assess the experimental outcomes against the prediction using JCA model for both SAA and TLA. Errors between the observed and predicted SAA for WH-1, WH-2, WH-3, WH-4, and WH-5 were 0.0163, 0.0084, 0.0082, 0.0417, and 0.0982 respectively. The average error of the SAA of all samples is 0.0346. The corresponding TLA errors were 0.0930, 0.1711, 0.0444, 0.1416, and 0.3631. The average error of the TLA of all samples is 0.1626. Compared to the values obtained from statistical models investigated in the previous subsection, the error of the values obtained using the JCA model is higher. However, the JCA model provides a comprehensive prediction of the SAC and TL spectrum, making it more versatile in predicting other parameters such as the Noise Reduction Coefficient (NRC) and sound absorption at frequencies higher than 2500 Hz. For the SAA of materials with an air gap, the JCA model predicts the SAA with higher accuracy than the statistical models. The average errors for SAAs with 20 mm and 40 mm air gaps are 0.0318 and 0.0440, respectively. These errors are significantly lower than those of the statistical models, which are 0.1892 and 0.2074 for SAAs with 20 mm and 40 mm air gaps, respectively.

3.6. The empirical model for sound absorption coefficient

The Johnson-Champoux-Allard (JCA) model, requiring five parameters to predict the sound absorption coefficient (SAC), may not always be practical for use when sample information is limited. In contrast, empirical models are more suitable as they demand fewer independent variables to determine outcomes like the SAC. The Delany-Bazley (D-B) model is favored for its simplicity and has been widely used to predict the SAC spectrum; it was originally developed by fitting the SAC spectra of various glass fiber specimens. Additionally, the Garai-Pompoli (G-P) model, developed from data on polyester fiber, also provides a reliable empirical method for predicting the SAC spectrum of fibrous-type absorbers. The primary requirement for predicting the SAC spectra with this empirical model is the airflow resistivity of the porous absorber. This resistivity can be calculated from the sample density using Eq. 15.

However, the applicability of the D-B and G-P models may not extend to all sample types. It is particularly intriguing to explore whether these models can accurately predict the SAC spectra of water hyacinth composites in this study. The airflow resistivity values listed in Table 1 are employed to estimate a new empirical model for the SAC, which is based on a power-law relationship derived from the D-B model, with the general expressions outlined in Eqs. 16 and 17 (Chanlert et al., 2023; Delany and Bazley, 1970; Soltani et al., 2020). The SAC of the predictive model can be accurately estimated by substituting the values from these equations into Eq. 18.

$$Z_c = \rho_0 c_0\left[1 + C_1\left(\frac{\rho_0 f}{\sigma}\right)^{-C_2} - jC_3\left(\frac{\rho_0 f}{\sigma}\right)^{-C_4}\right] \tag{16}$$

$$K_c = \omega / c_0\left[1 + C_5\left(\frac{\rho_0 f}{\sigma}\right)^{-C_6} - jC_7\left(\frac{\rho_0 f}{\sigma}\right)^{-C_8}\right] \tag{17}$$

$$Z_s = -jZ_c\cot(K_c d) \tag{18}$$

The optimal values for parameters C_1 to C_8 were determined using the least-square method, as detailed in Eqs. 16 - 18. SAC spectra from five distinct samples (WH-1 to WH-5) were employed in the reverse estimation of our new model (WH model) for water hyacinth composites, with the parameters displayed in Table 4. Additionally, the Garai-

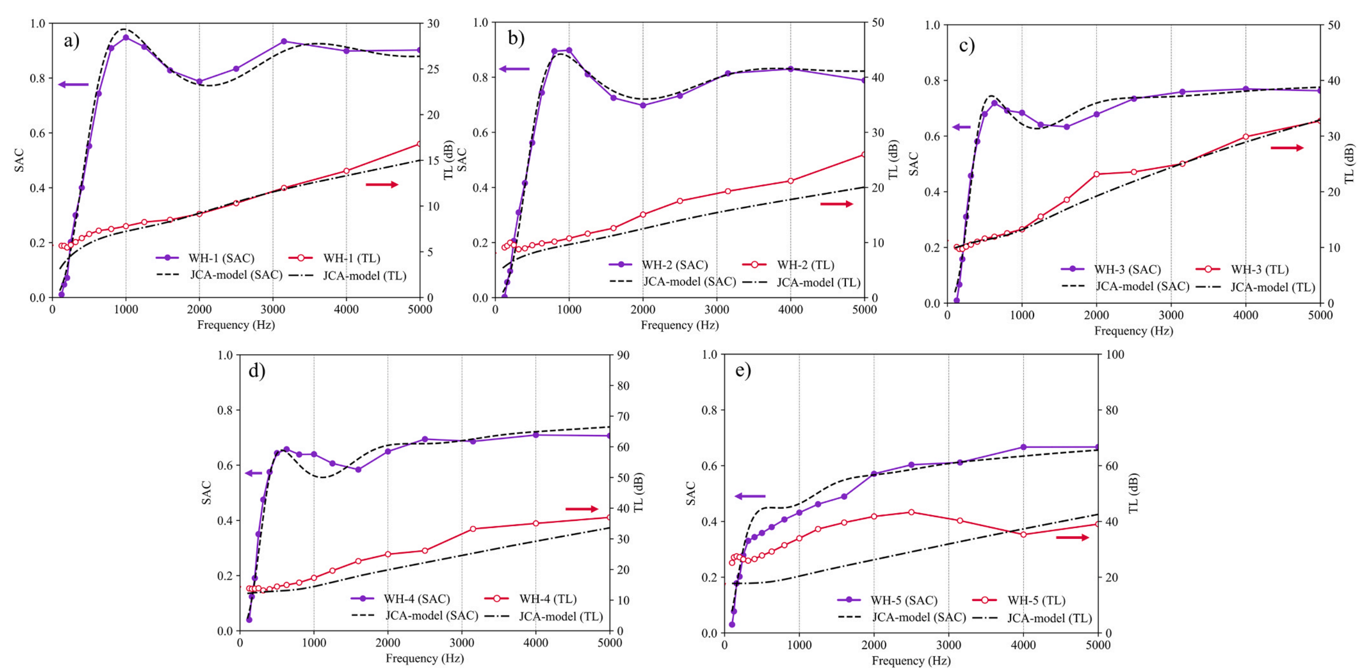

Fig. 9. Experimental and calculated SAC and TL spectra using JCA model for a) WH-1, b) WH-2, c) WH-3, d) WH-4, and e) WH-5.

Table 4
The comparison between eight parameters of the D-B, G-P and the new empirical model.

Model	C_1	C_2	C_3	C_4	C_5	C_6	C_7	C_8
Delany-Bazley	0.057	0.754	0.087	0.732	0.098	0.700	0.189	0.595
Garai-Pompoli	0.078	0.623	0.074	0.660	0.121	0.530	0.159	0.571
New model	0.285	0.598	-0.865	0.159	-3.555	0.069	1.313	0.153

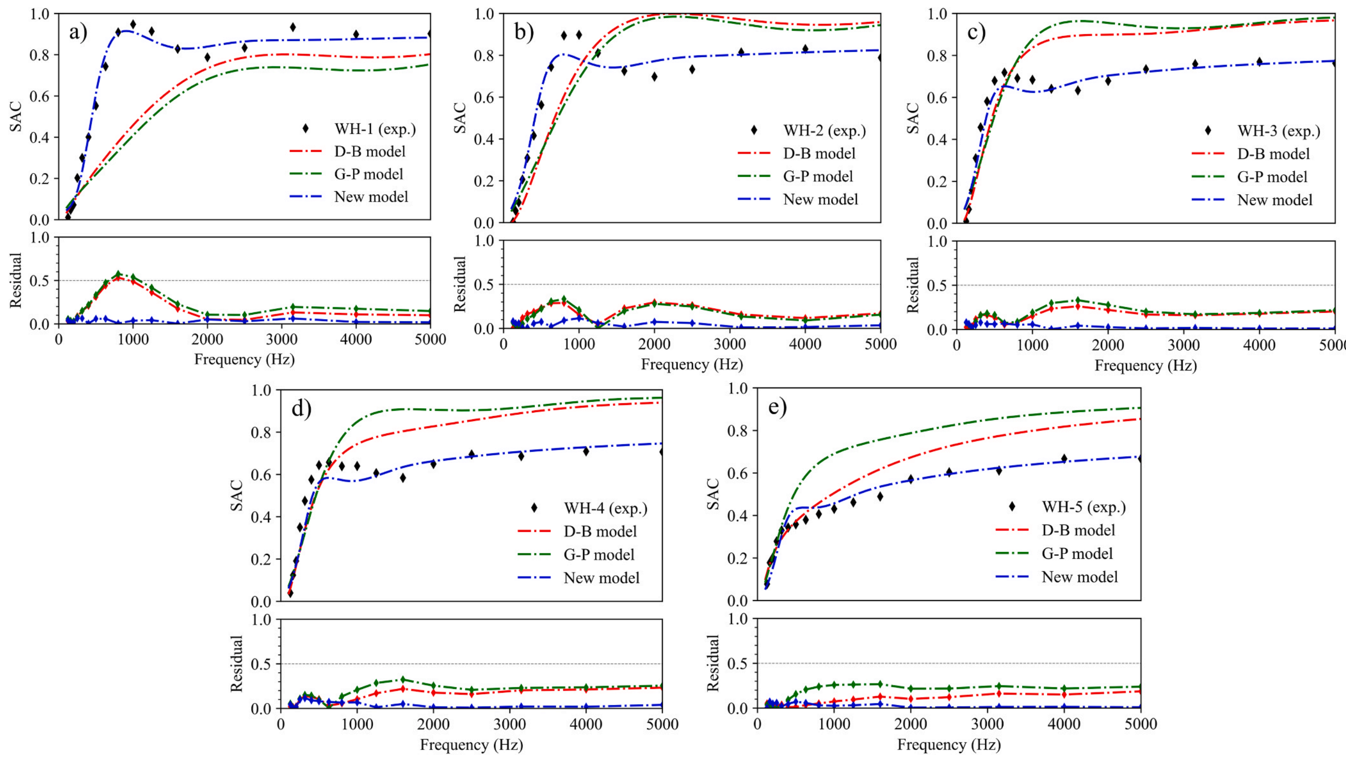

Fig. 10. Experimental and calculated SAC spectra using the empirical D-B, G-P and the new model for a) WH-1, b) WH-2, c) WH-3, d) WH-4, and e) WH-5.

Table 5
SAA values of composites of water hyacinth and other natural fibers with 40 mm thickness.

ρ (kg/m^3)	Natural fiber composites	σ (Pa·s·m^{-2})	SAA			Reference
			Exp.	DB	WH	
118	Water hyacinth	2824	0.63	0.39 (0.39)	0.63 (0.01)	Current study
100	Sugarcane baggasse	1823	0.42	0.33 (0.21)	0.61 (0.45)	(Mehrzad et al., 2022)
150	Kenaf	3230	0.50	0.40 (0.19)	0.62 (0.26)	(Halashi et al., 2024)
197	Water hyacinth	42061	0.58	0.62 (0.07)	0.55 (0.05)	Current study
200	Sugarcane baggasse	5647	0.64	0.47 (0.26)	0.64 (<0.01)	(Mehrzad et al., 2022)
200	Kenaf	5740	0.61	0.46 (0.22)	0.64 (0.05)	(Taban et al., 2020)
225	Luffa	7260	0.68	0.50 (0.26)	0.64 (0.06)	(Halashi et al., 2024)

The values in parentheses contain the errors between the observed (Exp.) and predicted SAA.

Pompoli model, developed from data on polyester fiber (Garai and Pompoli, 2005), serves as another reliable empirical method for predicting the SAC spectrum of fibrous-type absorbers. The parameters for both the Delany-Bazley (Delany and Bazley, 1970; Soltani et al., 2020) and Garai-Pompoli (Garai and Pompoli, 2005) models are listed in Table 4, and the SAC spectra predicted by these three models are illustrated in Fig. 10.

The errors between the SAAs predicted by D-B and G-P models and experimental results across all samples (WH-1 to WH-5) were 0.1406 and 0.2316, respectively. In contrast, the newly developed model (WH model) demonstrated a significantly error of 0.0377 for the same samples. Comparatively, the error of the estimation using D-B and G-P models are approximately 4 and 7 times higher than those of the new model, respectively. This substantial reduction in error values suggests that the new model provides a much higher accuracy than the established models in predicting the sound absorption spectrum of water hyacinth composites under specific conditions. It should be noted that the model's predictions are most accurate when applied to panels that are 40 mm thick and have an airflow resistivity ranging between 2824 and 134251 Pa·s·m^{-2}. The development of this empirical model significantly enhances the ability of researchers to predict the SAC of water hyacinth composites rapidly and accurately, facilitating more efficient and effective use of these materials in practical applications.

3.7. Comparative analysis

Table 5 provides a detailed comparison of the Sound Absorption Average (SAA) of water hyacinth composites studied in the current research with other natural fiber composites from previous studies, all having a uniform thickness of 40 mm. This analysis highlights the differences in sound absorption characteristics across various natural fibers and densities, alongside the performance of predictive models.

For low-density samples (100 $\sim$ 150 kg/m^3), water hyacinth composites exhibit similar airflow resistivity (AFR) to other natural fibers. Specifically, the AFR for water hyacinth at 118 kg/m^3 is 2824, comparable to sugarcane baggasse in 1823 for 100 kg/m^3 and kenaf at 3230 for 150 kg/m^3. In terms of sound absorption, water hyacinth composites demonstrate a higher SAA (0.63) compared to sugarcane baggasse (0.42) and kenaf fiber (0.50). This indicates superior sound absorption properties of water hyacinth at lower densities. Conversely, at higher densities ($\sim$200 kg/m^3), water hyacinth composites exhibit much higher AFR (42061) compared to sugarcane baggasse (5647) and kenaf (5740). This significant difference is attributed to the larger diameter of water hyacinth fibers, resulting in a lower surface area and reduced porosity. The reduced porosity restricts airflow, leading to higher airflow resistivity. Consequently, the SAA for high-density water hyacinth composites (0.58) is lower than that of sugarcane baggasse (0.64) and kenaf fiber (0.61).

The WH model, developed in this study, shows varying predictive accuracy. For low-density samples, the WH model does not predict the SAA of sugarcane baggasse and kenaf fiber as accurately as the Delany-Bazley model, with errors of 0.45 and 0.26, respectively. However, for high-density samples, the WH model outperforms the Delany-Bazley model in predicting SAA, with overall errors around 0.05–0.06, compared to the Delany-Bazley model's errors in the range of 0.2–0.3. Notably, the Delany-Bazley model can predict the SAA of high-density water hyacinth samples with minimal error, such as 0.07 % for a sample with a density of 197 kg/m^3. The WH model was derived from fitting the SAC spectra of water hyacinth fiber with limited ranges of airflow resistivity and sample thickness. Its versatility would improve by incorporating SAC spectra from other fibers and various sample thicknesses. As shown in Table 5, the WH model predicts SAA for high-density samples better than the traditional Delany-Bazley model. This suggests its potential to be developed into a more general model capable of predicting SAC spectra for various materials, similar to the Delany-Bazley and Garai-Pompoli models.

Since, in this study, a manual method was used to extract fibers from water hyacinth stalks, which limits the ability to achieve finer fibers. To obtain finer fibers, the most efficient method is to use a fiber extractor machine. This machine mechanically crushes the water hyacinth stalks into finer strands through repeated crushing and refining processes. Specifically, a fiber extractor machine, such as a decorticator, can be utilized. This machine operates by breaking down the fibrous material through mechanical impact or grinding, resulting in finer fibers. Implementing such machinery would significantly enhance the fineness of the fibers.

This study highlights the impressive sound absorption capabilities of water hyacinth, a floating river weed, underscoring its potential in acoustic applications. Utilizing water hyacinth offers several benefits for environmental sustainability. Firstly, water hyacinth is listed among the "100 of the World's Worst Invasive Alien Species," causing negative effects on local biodiversity (Lowe et al., 2000). Controlling invasive species in natural habitats is crucial for slowing down biodiversity loss, as invasive species are a major concern in several national and international biodiversity conservation policies (Keller et al., 2011). Moreover, removing water hyacinth from water bodies can improve water quality by promoting better flow and reducing environmental impact (Viriyavisuthisakul et al., 2018). Therefore, using water hyacinth for bio-based materials may help control its population and mitigate the invasive species problem. Secondly, the natural fiber extracted from water hyacinth is not only cost-effective and easy to recycle but also exhibits strong biodegradable properties. Soil biodegradation tests have shown that water hyacinth biocomposites experience approximately 30–50 % weight loss in 15 days, indicating their biodegradability (Syafri et al., 2019a, 2019b). This contrasts with widely used industrial composites like polyurethane and fiberglass, which generally take over 20 years and several years to degrade, respectively (Hausrath and Longobardo, 2010; Pellizzi et al., 2014). Additionally, the natural fiber can be transformed into various products such as bio-composites, supercapacitors, biomass energy sources, and fertilizers (Guna et al., 2017), making it applicable for various environmentally friendly products. In our experiment, we used polyvinyl alcohol (PVA) as a binder due to its biodegradability (Chiellini et al., 2003; Rahman and Goswami, 2022). PVA can degrade by 75 % within 46 days, making it an environmentally friendly polymer. However, high concentrations of PVA in industrial wastewater can pose risks to marine life. Research indicates that long-chain PVA can be broken down into smaller molecules by enzymes produced by microorganisms like bacteria and further degraded into acetic acid, hydrogen, and carbon dioxide (Rahman and Goswami, 2022). These aspects suggest that while PVA offers certain environmental advantages, its complete impact requires careful consideration and management to ensure sustainability. Therefore, water hyacinth composite material presents a promising eco-friendly alternative for developing sound absorption products, offering benefits for both environmental sustainability and material innovation. However, due to the biodegradability of natural fibers, there are concerns regarding their durability and stability under thermal or chemical conditions. Glass wool and polyurethane foam have been in use for a long time (Aso and Kinoshita, 1965; Imai and Asano, 1982), demonstrating their suitability for various conditions (Ehsan Samaei et al., 2023; Lee and Jung, 2019) related to construction and building materials. Although natural fibers like water hyacinth can be made into bio-based composites, there is still a long way to go before they can be used at a mass production level.

4. Conclusions

This study provides a detailed analysis of the sound absorption and insulation properties of natural fiber composites made from water hyacinth fibers.

1. Among the samples tested, WH-1, with a density of 118 kg/m^3, displayed the highest Sound Absorption Average (SAA) at 0.63, whereas WH-5, the sample with the highest density at 282 kg/m^3, showed the greatest Transmission Loss Average (TLA) at 32.5 dB. The data reveals that as sample density increases, SAA tends to decrease, while TLA increases.
2. The analysis of variance (ANOVA) demonstrated that both sample density and air gap exert a linear influence on the value of SAA, while only sample density exhibits a quadratic influence on SAA at a 95 % confidence interval. Similarly, sample density shows both linear and quadratic influences on TLA with a confidence interval above 95 %.
3. In terms of the JCA model parameters, airflow resistivity was found to increase with higher density, whereas all other parameters—including open porosity and viscous/thermal characteristic lengths—showed an inverse relationship with density. The new empirical model (WH model) has also been developed for predicting the SAC, with an average error of 0.0377, which is 4–7 times lower than the error of established models such as the Delany-Bazley and Garai-Pompoli models.

4. Future research will explore a broader range of variables, including variations in sample thickness and modifications to fiber strand size. **Types of Binder**—Identifying binders that enhance bonding without compromising acoustic properties. **Water Repellent Coatings**—Investigating the effects of water repellent coatings on acoustic properties and durability. **Long-Term Durability and Environmental Impact**—Assessing resistance to environmental degradation and sustainability. **Hybrid Material Development**—Exploring the combination of water hyacinth fibers with other natural or synthetic materials for improved performance characteristics. **Thermal Stability**—Studying the thermal stability of water hyacinth fibers to determine their suitability for different environmental conditions.

CRediT authorship contribution statement

Maenila Srisawas: Writing – review & editing, Visualization, Methodology, Investigation, Formal analysis, Data curation, Conceptualization. **Thanate Kerdkaew:** Writing – review & editing, Writing – original draft, Visualization, Validation, Supervision. **Purintorn Chanlert:** Writing – review & editing, Writing – original draft, Visualization, Validation, Supervision, Software, Resources, Project administration, Methodology, Investigation, Funding acquisition, Formal analysis, Data curation, Conceptualization.

Declaration of Competing Interest

The authors declare that they have no known competing financial interests or personal relationships that could have appeared to influence the work reported in this paper.

Data availability

Data will be made available on request.

Acknowledgements

We are thankful to the Faculty of Science and Technology at Songkhla Rajabhat University, Thailand, for providing us with essential scientific tools and equipments.

References

Allard, J.F., Atalla, N., 2009. Propagation of Sound in Porous Media, 1st ed. Wiley, Hoboken, New Jersey, USA.
Allard, J.F., Champoux, Y., 1992. New empirical equation for sound propagation in rigid frame fibrous materials. J. Acoust. Soc. Am. 91, 3346–3353. https://doi.org/10.1121/1.402824.
Aso, S., Kinoshita, R., 1965. Sound absorption coefficient of glass wool. T649–T653 J. Text. Mach. Soc. Jpn. - Trans. - 18. https://doi.org/10.4188/transjtmsj1965b.18.t649.
ASTM-E1050, 1990. Standard test method for impedance and absorption of acoustical materials using a tube, two microphones and a digital frequency analysis system, American Society for Testing of Materials. ASTM International, West Conshohocken, Pennsylvania, United States. https://doi.org/10.1520/E1050-12.
ASTM-E2611, 2019. Standard Test Method for Normal Incidence Determination of Porous Material Acoustical Properties Based on the Transfer Matrix Method, American Society for Testing of Materials. ASTM International, West Conshohocken, Pennsylvania, United States. https://doi.org/10.1520/E2611-19.
Bardot, A., Brouard, B., Allard, J.F., 1996. Frame decoupling at low frequency in thin porous layers saturated by air. J. Appl. Phys. 79, 8223–8229. https://doi.org/10.1063/1.362462.
Berardi, U., Iannace, G., 2017. Predicting the sound absorption of natural materials: best-fit inverse laws for the acoustic impedance and the propagation constant. Appl. Acoust. 115, 131–138. https://doi.org/10.1016/j.apacoust.2016.08.012.
Cai, Z., Li, X., Gai, X., Zhang, B., Xing, T., 2020. An empirical model to predict sound absorption ability of woven fabrics. Appl. Acoust. 170, 107483 https://doi.org/10.1016/j.apacoust.2020.107483.
Cai, X., Yang, J., Hu, G., 2015. Optimization on microlattice materials for sound absorption by an integrated transfer matrix method. EL334–EL339 J. Acoust. Soc. Am. 137. https://doi.org/10.1121/1.4916791.
Castoldi, R. de S., Souza, L.M.S. de, de Andrade Silva, F., 2019. Comparative study on the mechanical behavior and durability of polypropylene and sisal fiber reinforced concretes. Constr. Build. Mater. 211, 617–628. https://doi.org/10.1016/J.CONBUILDMAT.2019.03.282.
Champoux, Y., Allard, J.F., 1991. Dynamic tortuosity and bulk modulus in air-saturated porous media. J. Appl. Phys. 70, 1975–1979. https://doi.org/10.1063/1.349482.
Champoux, Y., Stinson, M.R., 1992. On acoustical models for sound propagation in rigid frame porous materials and the influence of shape factors. J. Acoust. Soc. Am. 92, 1120–1131. https://doi.org/10.1121/1.405281.
Chanlert, P., Jintara, A., Manoma, W., 2022a. Comparison of the sound absorption properties of acoustic absorbers made from used copy paper and corrugated board. Bioresources 17, 5612–5621. https://doi.org/10.15376/biores.17.4.5612-5621.
Chanlert, P., Manoma, W., Jintara, A., Kerdkaew, T., Sutthibutpong, T., 2023. Experimental and semi-phenomenological investigation on sound absorption performance of natural granular sound absorber: a case study on rice bran composites. Chiang Mai J. Sci. 50, 1–17. https://doi.org/10.12982/CMJS.2023.015.
Chanlert, P., Ruamcharoen, P., Kerdkaew, T., 2024. Exploring the sound absorption and sound insulation capabilities of natural fiber composites: nipa palm peduncle fiber. Chiang Mai J. Sci. 51, 1–11. https://doi.org/10.12982/CMJS.2024.034.
Chanlert, P., Tongyoo, S., Rordrak, C., 2022b. Effects of urea–formaldehyde and polyvinyl acetate adhesive on sound absorption coefficient and sound transmission loss of palmyra palm fruit fiber composites. Appl. Acoust. 198, 108984 https://doi.org/10.1016/j.apacoust.2022.108984.
Chiellini, E., Corti, A., D'Antone, S., Solaro, R., 2003. Biodegradation of poly (vinyl alcohol) based materials. Prog. Polym. Sci. 28, 963–1014. https://doi.org/10.1016/S0079-6700(02)00149-1.
Dehdashti, Z., Soltani, P., Taban, E., 2024. Utilizing discarded face masks to fabricate sustainable high-performance panels for enhanced building thermal and acoustic comfort. J. Clean. Prod. 446 https://doi.org/10.1016/j.jclepro.2024.141304.
Delany, M.E., Bazley, E.N., 1970. Acoustical properties of fibrous absorbent materials. Appl. Acoust. 3, 105–116. https://doi.org/10.1016/0003-682X(70)90031-9.
Doutres, O., Atalla, N., Osman, H., 2015. Transfer matrix modeling and experimental validation of cellular porous material with resonant inclusions. J. Acoust. Soc. Am. 137, 3502–3513. https://doi.org/10.1121/1.4921027.
Ehrig, T., Dannemann, M., Luft, R., Adams, C., Modler, N., Kostka, P., 2020. Sound transmission loss of a sandwich plate with adjustable core layer thickness. Materials 13, 1–10. https://doi.org/10.3390/ma13184160.
Ehsan Samaei, S., Berardi, U., Asilian Mahabadi, H., Soltani, P., Taban, E., 2023. Optimization and modeling of the sound absorption behavior of polyurethane composite foams reinforced with kenaf fiber. Appl. Acoust. 202, 109176 https://doi.org/10.1016/J.APACOUST.2022.109176.
Fattahi, M., Taban, E., Soltani, P., Berardi, U., Khavanin, A., Zaroushani, V., 2023. Waste corn husk fibers for sound absorption and thermal insulation applications: a step towards sustainable buildings. J. Build. Eng. 77, 107468 https://doi.org/10.1016/J.JOBE.2023.107468.
Garai, M., Pompoli, F., 2005. A simple empirical model of polyester fibre materials for acoustical applications. Appl. Acoust. 66, 1383–1398. https://doi.org/10.1016/j.apacoust.2005.04.008.
Golzari, M., Jafari, A.A., 2018. Sound transmission loss through triple-walled cylindrical shells with porous layers. J. Acoust. Soc. Am. 143, 3529–3544. https://doi.org/10.1121/1.5041270.
Guna, V., Ilangovan, M., Anantha Prasad, M.G., Reddy, N., 2017. Water hyacinth: a unique source for sustainable materials and products. ACS Sustain Chem. Eng. 5, 4478–4490. https://doi.org/10.1021/acssuschemeng.7b00051.
Halashi, K., Taban, E., Soltani, P., Amininasab, S., Samaei, E., Moghadam, D.N., Khavanin, A., 2024. Acoustic and thermal performance of luffa fiber panels for sustainable building applications. Build. Environ. 247, 111051 https://doi.org/10.1016/J.BUILDENV.2023.111051.
Hausrath, R.L., Longobardo, A.V., 2010. High-strength glass fibers and markets. Fiber Glass Technol.: Energy-Friendly Compos. Appl. 197–225. https://doi.org/10.1007/978-1-4419-0736-3_5.
Hosseini Fouladi, M., Nor, M.J.M., Ayub, M., Leman, Z.A., 2010. Utilization of coir fiber in multilayer acoustic absorption panel. Appl. Acoust. 71, 241–249. https://doi.org/10.1016/j.apacoust.2009.09.003.
Hulme, P., Vilà, M., Nentwig, W., Pyšek, P., 2010. Are the aliens taking over? Invasive species and their increasing impact on biodiversity. in: Atlas of Biodiversity Risk. Pensoft, Sofia, pp. 132–133.
Imai, Y., Asano, T., 1982. Studies of acoustical absorption of flexible polyurethane foam. J. Appl. Polym. Sci. 27, 183–195. https://doi.org/10.1002/app.1982.070270120.
ISO-10534, 1998. Determination of sound absorption coefficient and impedance in impedance tubes: Part 2: Transfer-function method, Part 2: Transfer-function method. International Organization for Standardization, Geneva, Switzerland. https://doi.org/10.3403/BSENISO10534.
ISO-9053-1, 2018. Acoustics-Determination of airflow resistance-Part 1: Static airflow method. International Organization for Standardization, Geneva, Switzerland. https://doi.org/10.31030/2874934.
Johnson, D.L., Koplik, J., Dashen, R., 1987. Theory of dynamic permeability and tortuosity in fluid-saturated porous media. J. Fluid Mech. 176, 379. https://doi.org/10.1017/S0022112087000727.
Johnson, D.L., Koplik, J., Schwartz, L.M., 1986. New pore-size parameter characterizing transport in porous media. Phys. Rev. Lett. 57, 2564–2567. https://doi.org/10.1103/PhysRevLett.57.2564.
Keller, R.P., Geist, J., Jeschke, J.M., Kühn, L., 2011. Invasive species in Europe: ecology, status, and policy. Environ. Sci. Eur. 23, 1–17. https://doi.org/10.1186/2190-4715-23-23/FIGURES/1.
Kudo, Y., Kotani, M., Tomita, M., Aizawa, Y., 2009. Effects of rock wool on the lungs evaluated by magnetometry and biopersistence test. J. Occup. Med. Toxicol. 4, 1–7. https://doi.org/10.1186/1745-6673-4-5.

Lee, J., Jung, I., 2019. Tuning sound absorbing properties of open cell polyurethane foam by impregnating graphene oxide. Appl. Acoust. 151, 10–21. https://doi.org/10.1016/j.apacoust.2019.02.029.

Lei, L., Dauchez, N., Chazot, J.D., 2018. Prediction of the six parameters of an equivalent fluid model for thermocompressed glass wools and melamine foam. Appl. Acoust. 139, 44–56. https://doi.org/10.1016/j.apacoust.2018.04.010.

Lowe, S., Browne, M., Boudjelas, S., De Poorter, M., 2000. 100 of the World's Worst Invasive Alien Species A selection from the Global Invasive Species Database. Auckland.

Luu, H.T., Perrot, C., Monchiet, V., Panneton, R., 2017. Three-dimensional reconstruction of a random fibrous medium: geometry, transport, and sound absorbing properties. J. Acoust. Soc. Am. 141, 4768–4780. https://doi.org/10.1121/1.4989373.

Mahmood, Q., Siddiqi, M.R., Islam, E. ul, Azim, M.R., Zheng, P., Hayat, Y., 2005. Anatomical studies on water hyacinth (Eichhornia crassipes (Mart.) Solms) under the influence of textile wastewater. J. Zhejiang Univ. Sci. 6B, 991–998. https://doi.org/10.1631/jzus.2005.B0991.

Marbuah, G., Gren, I.-M., McKie, B., 2014. Economics of harmful invasive species: a review. Diversity 6, 500–523. https://doi.org/10.3390/d6030500.

Mehrzad, S., Taban, E., Soltani, P., Samaei, S.E., Khavanin, A., 2022. Sugarcane bagasse waste fibers as novel thermal insulation and sound-absorbing materials for application in sustainable buildings. Build. Environ. 211 https://doi.org/10.1016/j.buildenv.2022.108753.

Merve Küçükali Öztürk, Banu Nergis, Cevza Candan, Klara Kalinova, 2015. Effect of fiber diameter and air gap on acoustic performance of nanofibrous membrane. J. Chem. Chem. Eng. 9. https://doi.org/10.17265/1934-7375/2015.01.006.

Mvubu, M.B., Anandjiwala, R., Patnaik, A., 2019. Effects of air gap, fibre type and blend ratio on sound absorption performance of needle-punched non-woven fabrics. J. Eng. Fiber Fabr. 14 https://doi.org/10.1177/1558925019840874/ASSET/IMAGES/LARGE/10.1177_1558925019840874-FIG6.JPEG.

Norton, M.P., Karczub, D.G., 2003. Fundamentals of noise and vibration analysis for engineers, 2nd Edition, 2nd ed, Cambridge University Press. https://doi.org/10.3397/1.2721371.

Oladele, I.O., Michael, O.S., Adediran, A.A., Balogun, O.P., Ajagbe, F.O., 2020. Acetylation treatment for the batch processing of natural fibers: effects on constituents, tensile properties and surface morphology of selected plant stem fibers, 73 8 Fibers 2020 Vol. 8, 73. https://doi.org/10.3390/FIB8120073.

Park, S.H., Lee, M., Seo, P.N., Kang, E.C., Kang, C.W., 2020. Acoustical properties of wood fiberboards prepared with different densities and resin contents. Bioresources 15, 5291–5304. https://doi.org/10.15376/biores.15.3.5291-5304.

Pejchar, L., Mooney, H.A., 2009. Invasive species, ecosystem services and human well-being. Trends Ecol. Evol. 24, 497–504. https://doi.org/10.1016/j.tree.2009.03.016.

Pelegrinis, M.T., Horoshenkov, K.V., Burnett, A., 2016. An application of Kozeny-Carman flow resistivity model to predict the acoustical properties of polyester fibre. Appl. Acoust. 101, 1–4. https://doi.org/10.1016/j.apacoust.2015.07.019.

Pellizzi, E., Lattuati-Derieux, A., Lavédrine, B., Cheradame, H., 2014. Degradation of polyurethane ester foam artifacts: Chemical properties, mechanical properties and comparison between accelerated and natural degradation. Polym. Degrad. Stab. 107, 255–261. https://doi.org/10.1016/J.POLYMDEGRADSTAB.2013.12.018.

Rahman, L., Goswami, J., 2022. Poly(vinyl alcohol) as sustainable and eco-friendly packaging: a review. J. Packag. Technol. Res. 2022 7 (1 7), 1–10. https://doi.org/10.1007/S41783-022-00146-3.

Royal Irrigation Department of Thailand, 2023. Aquatic weeds eradication of Thailand in 2023: a progress report [in Thai]. Bangkok.

Sierra-Carmona, C.G., Hernández-Orduña, M.G., Murrieta-Galindo, R., 2022. Alternative uses of water hyacinth (Pontederia crassipes) from a sustainable perspective: a systematic literature review. Sustainability 14, 3931. https://doi.org/10.3390/su14073931.

Simón-Herrero, C., Peco, N., Romero, A., Valverde, J.L., Sánchez-Silva, L., 2019. PVA/nanoclay/graphene oxide aerogels with enhanced sound absorption properties. Appl. Acoust. 156, 40–45. https://doi.org/10.1016/j.apacoust.2019.06.023.

Soltani, P., Taban, E., Faridan, M., Samaei, S.E., Amininasab, S., 2020. Experimental and computational investigation of sound absorption performance of sustainable porous material: Yucca gloriosa fiber. Appl. Acoust. 157, 106999 https://doi.org/10.1016/j.apacoust.2019.106999.

Sukhawipat, N., Saengdee, L., Pasetto, P., Junthip, J., Martwong, E., 2022. Sustainable rigid polyurethane foam from wasted palm oil and water hyacinth fiber composite—a green sound-absorbing material. Polymers 14. https://doi.org/10.3390/polym14010201.

Syafri, E., Jamaluddin, Wahono, S., Irwan, A., Asrofi, M., Sari, N.H., Fudholi, A., 2019a. Characterization and properties of cellulose microfibers from water hyacinth filled sago starch biocomposites. Int J. Biol. Macromol. 137, 119–125. https://doi.org/10.1016/J.IJBIOMAC.2019.06.174.

Syafri, E., Sudirman, Mashadi, Yulianti, E., Deswita, Asrofi, M., Abral, H., Sapuan, S.M., Ilyas, R.A., Fudholi, A., 2019b. Effect of sonication time on the thermal stability, moisture absorption, and biodegradation of water hyacinth (Eichhornia crassipes) nanocellulose-filled bengkuang (Pachyrhizus erosus) starch biocomposites. J. Mater. Res. Technol. 8, 6223–6231. https://doi.org/10.1016/J.JMRT.2019.10.016.

Taban, E., Amininasab, S., Soltani, P., Berardi, U., Abdi, D.D., Samaei, S.E., 2021. Use of date palm waste fibers as sound absorption material. J. Build. Eng. 41, 102752 https://doi.org/10.1016/j.jobe.2021.102752.

Taban, E., Soltani, P., Berardi, U., Putra, A., Mousavi, S.M., Faridan, M., Samaei, S.E., Khavanin, A., 2020. Measurement, modeling, and optimization of sound absorption performance of Kenaf fibers for building applications. Build. Environ. 180, 107087 https://doi.org/10.1016/J.BUILDENV.2020.107087.

Taban, E., Tajpoor, A., Faridan, M., Samaei, S.E., Beheshti, M.H., 2019. Acoustic Absorption Characterization and Prediction of Natural Coir Fibers. Acoust. Aust. 47, 67–77. https://doi.org/10.1007/s40857-019-00151-8.

Tanpichai, S., Biswas, S.K., Witayakran, S., Yano, H., 2019. Water hyacinth: a sustainable lignin-poor cellulose source for the production of cellulose nanofibers. ACS Sustain Chem. Eng. 7, 18884–18893. https://doi.org/10.1021/acssuschemeng.9b04095.

Uris, A., Llopis, A., Llinares, J., 1999. Effect of the rockwool bulk density on the airborne sound insulation of lightweight double walls. Appl. Acoust. 58, 327–331. https://doi.org/10.1016/S0003-682X(98)00065-6.

Viriyavisuthisakul, S., Sanguansat, P., Yamasaki, T., 2018. Water Hyacinth Segmentation for Aquatic Weed Elimination in Thailand. 2018 14th International Conference on Signal-Image Technology & Internet-Based Systems (SITIS). IEEE, pp. 253–257. https://doi.org/10.1109/SITIS.2018.00046.

Wembe, B.D., Wiryikfu, N.C., Ntamack, G.E., Kenmeugne, B., Tchotang, T., Rolland, D., Stanislas, T.T., 2023. Extraction and physicochemical and thermomechanical characterizations of water hyacinth fibers eichhornia crassipes. Int J. Polym. Sci. 2023 https://doi.org/10.1155/2023/6652978.

Xiang, H.F., Wang, D., Liua, H.C., Zhao, N., Xu, J., 2013. Investigation on sound absorption properties of kapok fibers. Chin. J. Polym. Sci. 31, 521–529. https://doi.org/10.1007/s10118-013-1241-8.

Yang, T., Hu, L., Xiong, X., Petrů, M., Noman, M.T., Mishra, R., Militký, J., 2020. Sound absorption properties of natural fibers: a review. Sustainability 12, 8477. https://doi.org/10.3390/su12208477.

Yang, Y., Li, B., Chen, Zhaofeng, Sui, N., Chen, Zhou, Xu, T., Li, Y., Fu, R., Jing, Y., 2017. Sound insulation of multi-layer glass-fiber felts: Role of morphology. Text. Res. J. 87, 261–269. https://doi.org/10.1177/0040517516629142.

Zhang, L., Zhang, W., Xin, F., 2023. Broadband low-frequency sound absorption of honeycomb sandwich panels with rough embedded necks. Mech. Syst. Signal Process 196. https://doi.org/10.1016/j.ymssp.2023.110311.